Available online at www.sciencedirect.com
ScienceDirect
Thin Solid Films 515 (2006) 1461 – 1469
thin solid films
www.elsevier.com/locate/tsf

Characterization and photocatalytic activity of nanostructured indium tin oxide thin-film electrode for azo-dye degradation

Mohammad Hossein Habibi [a,*], Nasrin Talebian [a], Jong-Ha Choi [b]

[a] Department of Chemistry, University of Isfahan, Isfahan, 81746-73441, Iran
[b] Department of Chemistry, Andong National University, Andong 760-749, South Korea

Received 18 July 2005; received in revised form 13 December 2005; accepted 10 April 2006
Available online 23 June 2006

Abstract

Photocatalytically active indium tin oxide thin film electrodes were prepared by electron beam evaporation technique onto a glass substrate having thickness 120 nm. Degradation of reactive dye yellow direct 42 has been performed using photoeletrocatalysis. A biased potential is applied across indium tin oxide photoelectrode illuminated by UV light. The best experimental conditions were found to be dye concentration 1.0×10^{-5} mol L^{-1}, pH 5.25 and 0.5 mol L^{-1} NaCl as supporting electrolyte when the photoelectrode was biased at +0.5 V versus saturated calomel electrode. The effects of other electrolytes, dye concentration, pH solution, electrode annealing temperature and applied potentials have been also investigated and are discussed. Several common inorganic salts Na_2SO_4, Na_2CO_3, $NaNO_3$ and NaCl were chosen to act as supporting electrolytes, which was added into the dye solution. It is shown that the charge-transfer resistance of photoanode can be calculated by the analysis of its electrochemical impedance spectroscopy, and the photoelectrocatalytic degradation rate of yellow direct 42 was inversely proportional to the value of charge-transfer resistance of photoelectrodes at different pH. The value of charge-transfer resistance is smaller, the higher its photoelectroactivity is.

Keywords: Photodegradation; Azo dye; Charge-transfer resistance; Indium tin oxide; Impedance

1. Introduction

In past decades, heterogeneous photocatalysis using titanium dioxide has attracted increasing attention in the field of environmental research for photodegradation of undesirable organics in aqueous phases [1,2]. Because two major problems, the recombination of the photogenerated charge carriers [3,4] and the filtration step of suspended particles after water treatment, the application of the external potential [5,6] and immobilization of TiO_2 onto inert support materials [7–9] can be used to improve the efficiency of process toward photodegradation of organic pollutants in wastewater. Although the dye concentration in wastewater is usually lower than those of many other chemical compounds, these dyes are visible even at very low concentrations. Azo dyes are the most widely used commercial reactive dyes. They represent about 50% of the worldwide production and correspond to a serious source of contamination considering that approximately 15% of the synthetic textile dyes are lost in waste streams during the manufacturing or processing operations [10].

Various physicochemical, advanced oxidation processes, biological processes and usually a combination of processes are applied to treat dyes to meet regulatory discharge limits [11]. However, some of these processes are limited due to the fact that many of the dyes are xenobiotic and non-biodegradable. Thus, there is a need for developing treatment technology, which is more effective in eliminating dyes from the waste stream at its source. Advanced oxidation processes based on the chemical, photochemical and photocatalytic production of hydroxyl radicals ($^{\bullet}OH$), which act as strong oxidizing agents, have emerged as a promising technology for the degradation of organic pollutants. An attractive way to increase the photocatalytic efficiency consists on introducing a biasing potential into this process and this is referred to photoelectrocatalysis. Photoelectrocatalysis takes advantage of the heterogeneous photocatalytic process by applying a biased potential across a photoelectrode on which the

* Corresponding author. Tel.: +98 311 7932401; fax: +98 311 6687396.
E-mail address: habibi@chem.ui.ac.ir (M.H. Habibi).

0040-6090/$ - see front matter © 2006 Elsevier B.V. All rights reserved.
doi:10.1016/j.tsf.2006.04.037

catalyst is supported. This configuration allows the more effective separation of photogenerated charges thereby increasing the lifetime of electron-hole pairs [12].

Although the indium tin oxide (ITO) electrode has a good potential as photoelectrode materials, it has been received relatively less attention in comparison with TiO_2, Fe_2O_3, ZnO and some other oxide electrodes. The ITO is a degenerate n-type semiconductor with a wide band gap and, consequently, shows high electrical conductivity and transmits the visible light [13]. The ITO thin films are very widely used as transparent conducting electrodes for solar cell, displays, organic light emitting diodes and other electro-optical devices [14,15] However, there is little information on the photoelectrochemical and photocatalytic properties of indium oxide [16]. A wide variety of physical and chemical methods were proposed to study the electrical properties of semiconductor electrodes in contact with liquid electrolyte. Among them, impedance spectroscopy is a valuable experimental tool because it provides information about charge transfer phenomena, double layer properties, carrier generation-recombination processes, etc. The results of impedance analysis are usually discussed in terms of equivalent circuits. The proposed equivalent circuits were combinations of resistors and capacitors (i.e. Debye elements) [17]. However, more recent studies revealed that, apart from the mentioned Debye elements, it is necessary to use constant-phase elements in equivalent circuits describing the semiconductor/electrolyte interface [18].

In this paper, we report the results of studying photoelectrochemical properties of nanostructured ITO electrodes toward degradation of an azo dye, yellow direct 42. Yellow direct 42 (Fig. 1) was selected as model dyeing pollutant because azo dyes are among the largest group of colorants used in a variety of industrials such as textile and paper [19].

2. Experiments

2.1. Preparation of ITO electrodes

An electron beam evaporation system was used for film deposition. The evaporation conditions were: (1) a vacuum of 4.2×10^{-3} Pa, (2) an accelerating voltage of 1–10 kV, (3) electron beam current 10–12 mA and the rate of evaporation were controlled within the range 0.1–0.25 nm s^{-1}. The thickness of thin film was controlled by using a quartz crystal thickness monitor, resulting in films having 120 nm. The target material was an ITO pellet (purchased from Merck) with a composition of In_2O_3: 89.75 wt.%, SnO_2: 9.82 and trace amount of other oxides, which are determined by X-ray fluorescence analysis CaO: 0.12, K_2O: 0.096, Fe_2O_3: 0.069, CuO: 0.069, Al_2O_3: 0.025, ZnO: 0.025 and UO_2: 0.026.

2.2. Analytical methods

The crystalline phase of ITO films annealed at different temperatures (350–550 °C) were characterized using X-ray diffractometer (XRD) technique with a D8 Advanced Bruker X-ray diffractometer at room temperature, with monochromated Cu K_α ($\lambda=1.54$ Å) in the scan range of 2θ between 4° and 100° with a step size of 0.03 (2θ s^{-1}). Measurements were taken under beam-acceleration conditions of 40 kV/35 mA. UV–Vis spectra of ITO electrodes were measured with a UV–Vis double-beam spectrophotometer Cary 500 scan. Atomic force microscopy (AFM) investigations were carried out using a Park Scientific atomic force microscope. Commercial sharpened tips of Si_3N_4 with tips smaller than 10 nm were employed. The AFM images were recorded under contact mode to obtain high resolution. The $\langle\sigma\rangle$ was reduced to 5 nm following laser illumination at 157 nm with laser fluence of 1 mJ cm^{-2} per pulse.

2.3. Photoelectrochemical (PEC) measurements and degradation experiments

PEC measurements and degradations were performed using a three-compartment electrochemical cell with a Pyrex window; 15 ml of solutions of contaminant were treated at constant concentration of supporting electrolyte. Reaction temperature was not controlled; it did not rise beyond 35 °C during a typical 4 h experiment. The pH value was monitored either; the experiments were performed at the different pH. The photoactive area of the anode (ITO) was 15 cm^2 and was illuminated by a 450 W high pressure Hg lamp as an UV light source (315–400 nm). The compartment containing the platinum counter-electrode of approximately the same area was not directly exposed to the UV illumination. The reference electrode was saturated calomel electrode (SCE), the SCE used as a reference, was placed close to the working electrode. A Potentiostat/Galvanostat Autolab model Eco Chimi B.V. controlled by the electrochemical software was used to bias the photoanode in the photoelectrocatalytic experiments and also to record the linear sweep voltammetry plots for measuring photocurrents. All electrochemical impedance spectroscopy (EIS) spectra were fitted to the electrical equivalent circuits using Zveiw program.

The concentration of reactive yellow direct 42 dye in the solution during photodegradation was monitored by measuring the absorbance of samples of the dye solution at controlled time using a UV–Vis spectrophotometer.

2.4. Characterization of ITO electrodes

The as-deposited ITO film was then annealed up to 550 °C. The ITO film was characterized by atomic force microscopy (AFM),

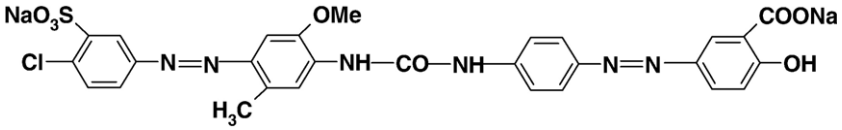

Fig. 1. Chemical structure of yellow direct 42.

XRD and UV–Vis spectrophotometry. Surface roughness and morphologies of ITO thin films were evaluated by AFM. In addition to the particle diameter, AFM image analysis also gives the values of surface roughness. The XRD patterns, obtained on X-ray diffractometer, were used to determine the identity of any phase present and their crystallite size. The crystallite size was calculated from X-ray line broadening analysis by Scherrer formula. UV–Vis spectra of films were obtained to follow the effect of annealing temperature on optical (transmittance percent and edge absorption shift) and transition electronic (E_g) properties.

2.5. Chemicals

The chemicals Na_2SO_4, Na_2CO_3, $NaNO_3$, NaCl and yellow direct azo dye were purchased from the suppliers and used without further purification.

3. Results and discussion

3.1. Characterization and selection of the ITO electrodes

3.1.1. X-ray diffraction analysis

XRD spectra show that the as-deposited films are amorphous. After annealing in atmosphere at 450 °C, the films showed the evidence of conversion from an amorphous state to a polycrystalline body-centered cubic In_2O_3 structure. When the XRD patterns are compared with those given in the JCPDS database (Card No. 06-0416), (222) preferred orientation is found. No phases corresponding to other tin compounds were detected (Fig. 2). Increasing the annealing temperature further improved the crystallinity. The average crystallite size of ITO films annealed at 450 °C and 550 °C, ca. 39 nm and 48 nm, respectively, was calculated using the line broadening methods and the equation proposed by Scherrer [20].

3.1.2. Optical properties

The optical properties of the films were investigated by UV–Vis spectrometer. Fig. 3 shows the optical transmission spectra for ITO films with a thickness of 120 nm annealed at different temperatures in the presence of air. As annealing temperature is increased, there is a general increase in transmission at all wavelengths, but there is also an increase in the steepness in the increase of the band edge absorption consistent with the improved crystallinity [13].

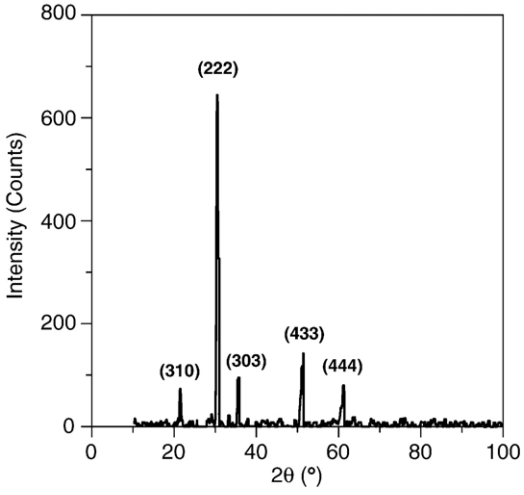

Fig. 2. XRD pattern for ITO thin film on glass annealed at 550 °C and thickness 120 nm.

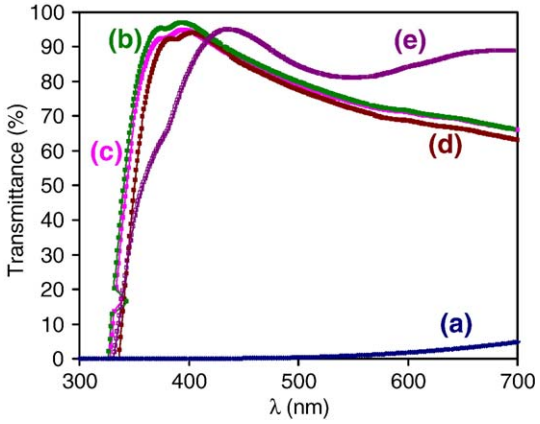

Fig. 3. UV–Vis spectra of ITO films of 120 nm thickness (a) as-deposited, annealed at (b) 250 °C, (c) 350 °C, (d) 450 °C and (e) 550 °C.

3.1.3. Surface morphology

Fig. 4 shows two-dimensional AFM images of ITO thin films annealed at (a) 450 °C and (b) 550 °C. The surface morphologies and roughness of films are obviously affected by annealing temperature. Both particle size and roughness of thin films are increased with annealing temperature.

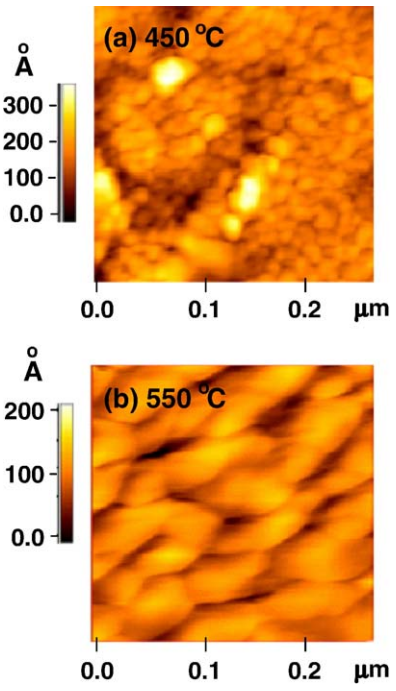

Fig. 4. Two-dimensional (a, b) AFM images of ITO thin film deposited on glass annealed at (a) 450 °C and (b) 550 °C.

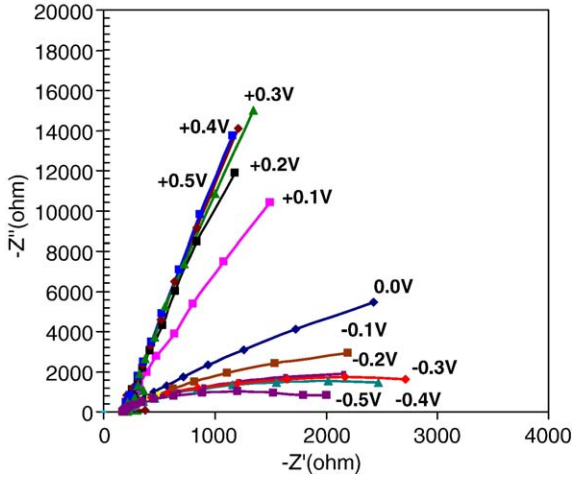

Fig. 5. Complex plane impedance plots (Nyquist plots) for ITO thin-film electrodes in 0.5 M NaCl at various potentials, pH 5.25.

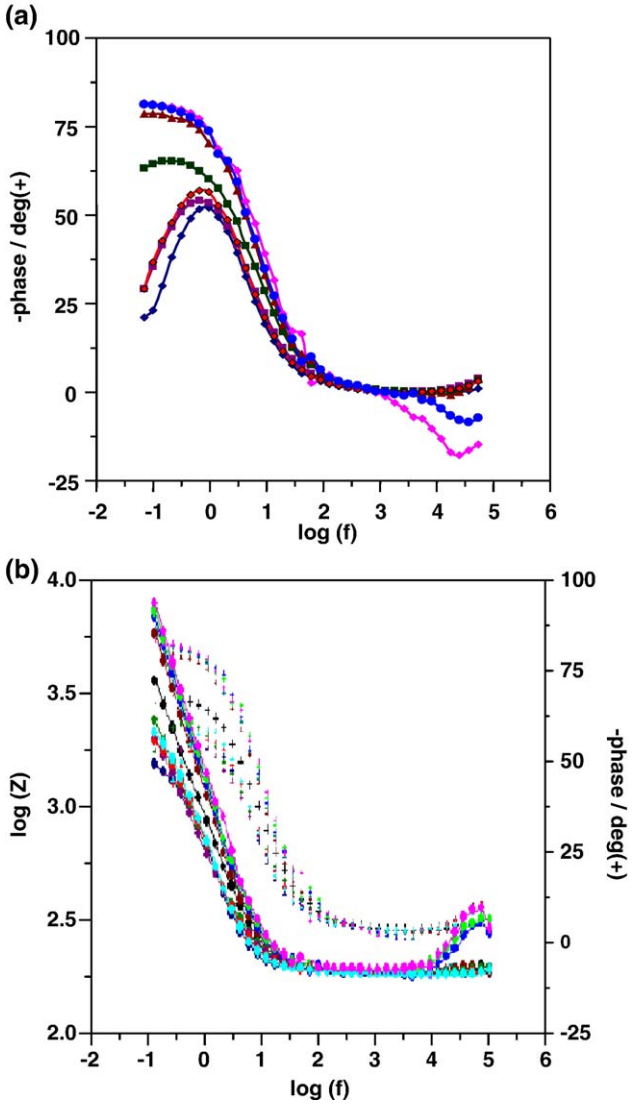

Fig. 6. Bode plots of ITO thin-film electrodes in 0.5 M NaCl at various potentials and pH 5.25.

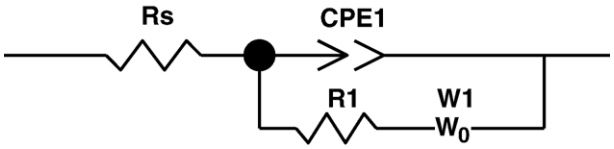

Fig. 7. The equivalent circuit used to fit impedance data.

3.1.4. Impedance spectroscopic characterization of the ITO film/electrolyte contact

In order to investigate the ITO film photoelectrochemical behavior, EIS was used. The main difficulty in analyzing EIS data and establishing the potential dependence of the capacity of the depletion layer is the choice of an adequate (possibly unique) equivalent circuit representing a semiconductor/solution interface. EIS spectra for ITO electrode (typical ones shown in Figs. 5 and 6) were analyzed using one equivalent circuit as shown in Fig. 7. R_s is the electrolyte and the probe serial resistance, R_1 is electrode resistance, W_o accounts for diffusion transport through the space charge layer and CPE1 is constant-phase elements. A typical result of the equivalent circuit analysis is presented in the form of a Mott-Schottky plot (Fig. 8). The flat band potential estimated at −0.065 V. Donor density calculated from the slop assuming a dielectric constant of 31 is 1.91×10^{20} cm^{-3} [19].

Figs. 5 and 6 show a typical EIS plot for ITO electrode. By using the equivalent circuit as above mentioned to fit the impedance data at different pH, it was found that the results were satisfactory (error less than 4%). The fitted results show there is a relation between the photodegradation rate of yellow direct 45 and resistance (R) of photocatalyst electrode at different pH. The photodegradation rate of yellow direct 45 is inversely proportional to resistance of photocatalyst at different pH. This can be explained by that, as the value of resistance increases with increasing the pH, the charges transfer across the interface between the semiconductor and solution becomes difficult, the recombination rate of photocarriers increases, thus the amount of photoactive species available reduces and the degradation rate of yellow direct

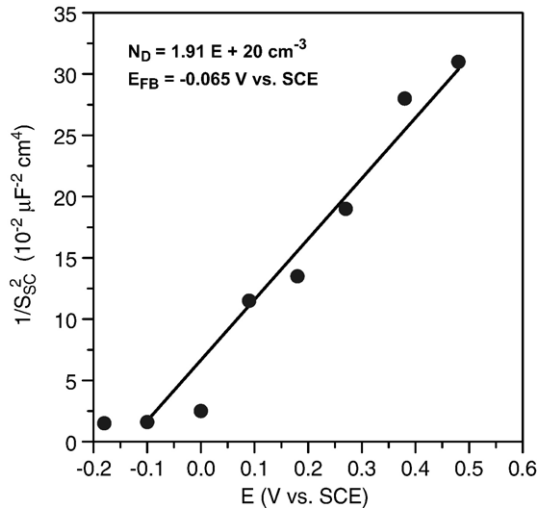

Fig. 8. High frequency region Mott-Schottky plot for ITO thin-film electrodes in 0.5 mol L^{-1} NaCl of pH 5.25 over potential range between −0.2 and 0.5 V vs. SCE.

45 decreases. The value of resistance is smaller, the higher the degradation rate of pollutant is, namely, the value of charge-transfer resistance reflects the activity of photocatalyst. Thus, it can be evaluated the photoelectrocatalytic activities of catalysts by the value of charge-transfer resistance. This is of interest due to at least not needing to carry out the experiments for the photo-degradation of pollutants.

Fig. 9 shows the impedance spectra (and electrode resistance) dependence on pH solution.

3.2. Degradation experiments

Three distinct conditions were investigated: (a) the photocatalytic treatment by using UV light without a bias potential, (b) the electrocatalytic treatment by biasing the electrode with +1.0 V (SCE) in dark conditions and (c) finally the photoelectrocatalytic treatment, i.e. using both UV light and +0.5 V (SCE) of bias potential. The comparative results are shown in Fig. 10.

The degradation process was monitored by UV–Vis spectroscopic measurement at λ=415 and 302 nm, in order to verify the

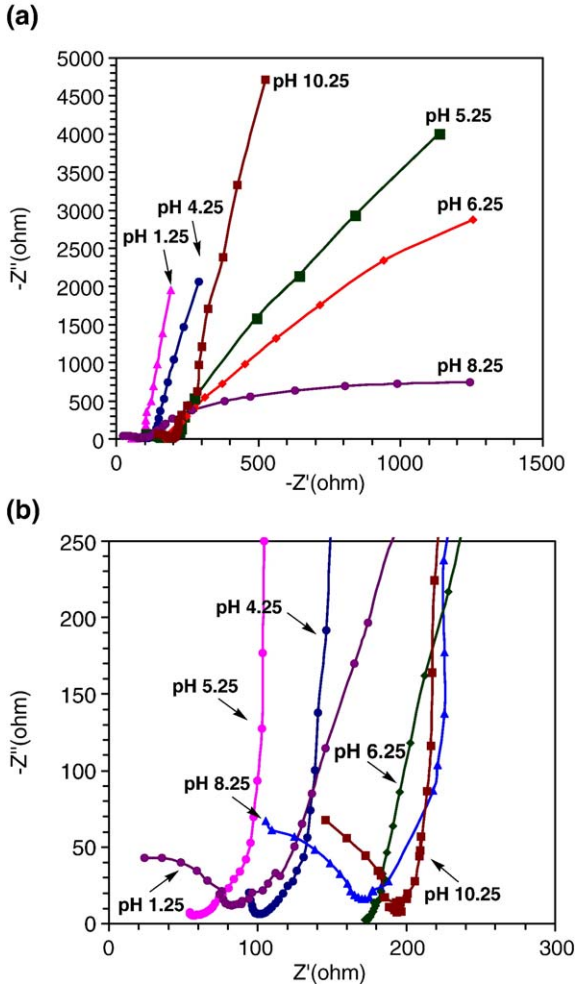

Fig. 9. (a) Impedance plots (Nyquist plots) for ITO thin-film electrode in 0.5 M NaCl at various pH, (b) the same plots magnified.

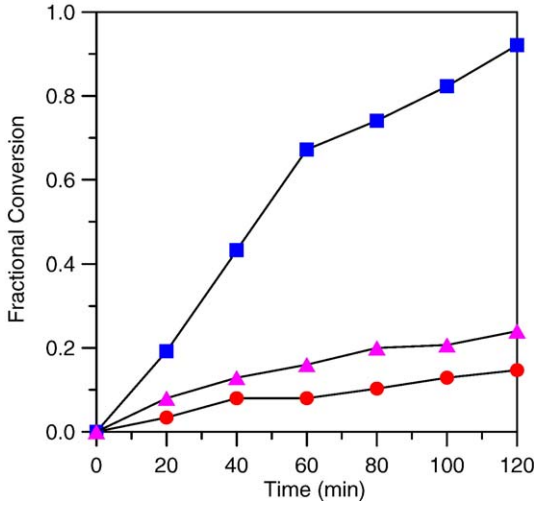

Fig. 10. Fractional conversion as a function of time for: (▲) the photocatalytic process using UV light, (●) applying E=+0.5 V and (■) with both UV light and E=+0.5 V. In all cases, dye concentration was 1×10^{-5} mol L^{-1} in 0.5 mol L^{-1} NaCl and pH 5.25.

break-down of the chromophoric group and modification of the aromatic character of the chemical structure in the dye molecule. Under photocatalytic conditions, about 23% of the dye solution was bleached within 120 min of irradiation (λ=415 nm) for yellow direct concentration 1×10^{-5} mol L^{-1} and pH 5.25. From discoloration measurements, a linear fit between $\ln(C_o/C)$ and irradiation time is obtained, suggesting that the color removal of the yellow direct dye follows a pseudo-first-order kinetics with apparent first-order constant of 4.8×10^{-3} min^{-1}. The signals obtained in the ultraviolet region were more persistent to the photochemical process, remaining almost unchanged up to reaction times of 120 min (λ=302 nm).

By applying a biasing potential of E_{app}=+0.5 V to the ITO thin-film photoanode, a bleaching of 100% at λ=415 nm and a degradation of 49% at λ=302 nm are obtained for azo dye.

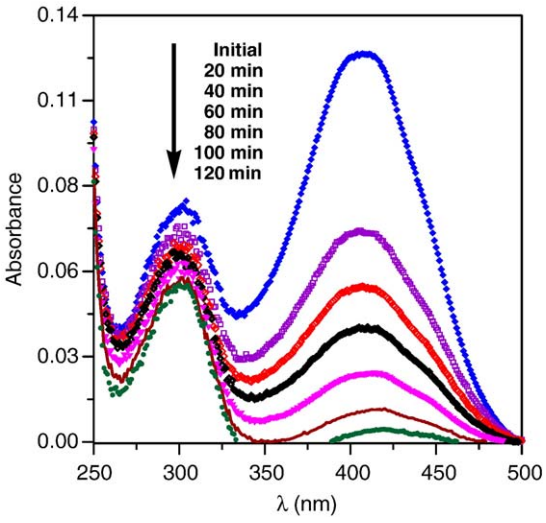

Fig. 11. A typical UV–Vis absorption spectra recorded at different time intervals for yellow direct 42 containing 0.5 M NaCl (yellow direct 42 1×10^{-5} mol L^{-1}, pH 5.25 potential vs. SCE, illumination, 450 W Hg lamp).

Also, the photoelectrodegradation leads to a linear plot of $\ln(C_o/C)$ versus time with a slope of 0.0102 min^{-1}, indicating that the photoelectrocatalytical degradation rate is at least two and half times faster than the photocatalytic process. Fig. 11 shows the changes in UV–Vis absorption spectra for yellow direct 42 solution after photoelectrochemical degradation for every 20 min intervals of a total irradiation time of 120 min in the presence of 0.5 M NaCl as supporting electrolyte.

The results obtained illustrate that under applied potential there is an improvement of the photocatalytic decomposition of the dye. By applying an anodic bias potential higher than the flat band potential of ITO electrode (−0.056 V vs. SCE), the competitive reactions of charge recombination (e^-/h^+) are minimized. A potential gradient within the photocatalyst film is provided at potentiostatic conditions to efficiently force the electrons to reach the counter electrode. Therefore, photogenerated holes can be trapped in the surface by H_2O/OH^- species to give rise to $^{\bullet}OH$ radicals, which are essential for promoting the efficient degradation of dyes. However, in most of electrochemically assisted photocatalytic experiments, the applied anodic bias potential is always lower than the oxidation potential of the organic pollutant so that no direct electro-chemical oxidation complicates the analysis of photocatalytic efficiency as shown in Fig. 10 [21].

The stability of ITO thin film were investigated using the same film over 10 times in the photoelectrochemical degradation of dye. The results showed that the efficiency ITO thin film in the photoelectrochemical degradation of dye remained almost unchanged.

The ITO film also showed excellent efficiency of photocatalytic degradation for azo dye compared to that of normal ITO micro-sized powder. The advantages of nanostructured ITO film include a higher photocatalytic activities and avoidance of separating solid–liquid phase.

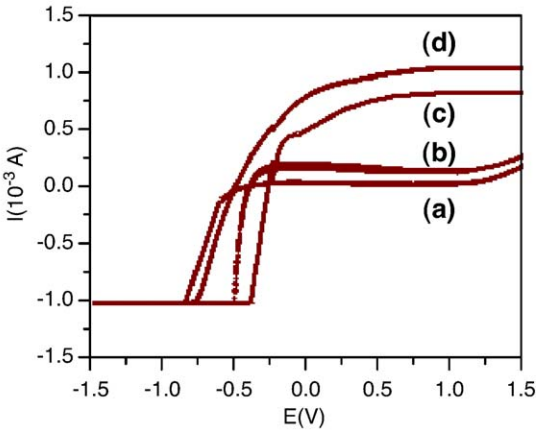

Fig. 12. Photocurrent–potential curves obtained for ITO thin-film electrodes for Na_2SO_4 (curve a), Na_2CO_3 (curve b), $NaNO_3$ (curve c) and NaCl (curve d) of the same concentration 0.5 mol L^{-1} under UV illumination (scan rate = 10 mV s^{-1} and pH 2.25).

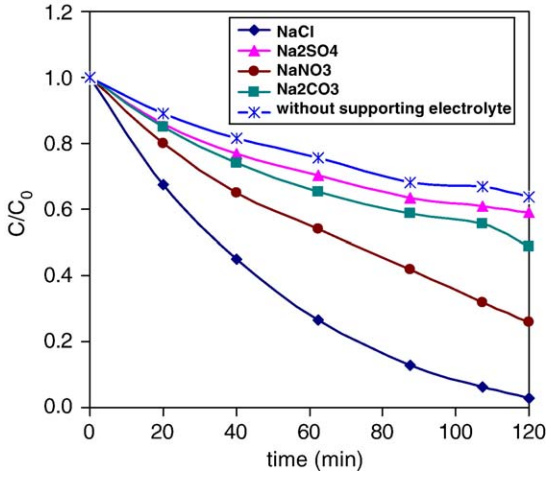

Fig. 13. The effect of various anions of supporting electrolyte in the photo degradation (1×10^{-5} M dye con., 0.5 M anions, +0.5 V potential and 450 W Hg lamp irradition).

3.3. Effect of annealing on photoactivity of ITO film electrode

The photoelectrochemical degradation of yellow direct 42 dye on ITO film electrodes under different annealing conditions are investigated. The dye degradation rates increase with the film annealing temperature from 0.0086 to 0.0102 min^{-1} for 350 to 550 °C, respectively. The observed increase in the dye degradation rate with ITO annealing temperature is most likely due to the changes in the surface structure and adhesion of films, especially for films annealed at higher temperatures. The annealing reduces the number of surface states in ITO and contributes to the decrease of the recombination rate of photo-generated electron-hole pairs. Thus, the ITO films used in further experiments were annealed at 550 °C.

3.4. Characteristics of the photoanode

Photocurrent associated with the ITO photoelectrodes under UV irradiation as a function of applied potential was investigated in aqueous solution of pH 5.25 in the presence of NaCl 0.5 mol L^{-1} by recording LSV curves. A profile of such curves is shown in curve (*d*) of Fig. 12. Typically, under UV–Vis irradiation, an n-type semiconductor electrode such as ITO produces a high anodic photocurrent at potentials positive to the flat band potential.

3.5. Effect of supporting electrolyte on dye degradation rate

To select a suitable supporting electrolyte, the photoelectrochemical degradation experiments were carried out in different supporting electrolytes, including NaCl, $NaClO_4$, $NaNO_3$ and Na_2SO_4. The results are shown in Fig. 13. The same concentration (0.5 M) of anion in all electrolytes was used. The highest degradation rate is observed in the chloride medium.

Fig. 13 shows a great influence of the anions of supporting electrolyte in the photodegradation process. Significant enhancement in the photodegradation rate occurred in chloride medium, while the opposite effect is observed in sulphate and

Table 1
Rate constants of various ions with $^{\bullet}OH$ radicals

Anions	Rate constants (s^{-1})	References
NO_3^-	1.4×10^8	[23]
Cl^-	4.3×10^9	[24]
HCO_3^-	8.5×10^{-6}	[24]
CO_3^{2-}	3.9×10^8	[24]
SO_4^{2-}	1.0×10^{10}	[25]
HSO_4^-	3.5×10^5	[26]

carbonate medium. It is well known that photodegradation started with the formation of $^{\bullet}OH$ radical. In an electro-chemical system the formation of this highly strong oxidizing agent resulted from oxidation of molecular water or hydroxyl ion on the surface of the electrode (SC for semiconductor), which can be represented by the following equations.

$$SC + h_{vb}^+ + OH^- \rightarrow SC + {}^{\bullet}OH \quad (1)$$

$$SC + h_{vb}^+ + H_2O \rightarrow SC + H^+ + {}^{\bullet}OH \quad (2)$$

In chloride containing medium another oxidizing radical, $Cl^{\bullet}$ is formed through a competing electrochemical process on the electrode surface.

$$SC + h_{vb}^+ + Cl^- \rightarrow SC + Cl^{\bullet} \quad (3)$$

The probability for chloride ions to react on the ITO surface to produce the radical is relatively low due to the large quantitative differences between water and chloride ions in the solution. Thus, it may be expected that chloride ion is more favorable in terms of competition to be adsorbed on the electrode surface compared to water or hydroxyl ions. This is attributed to water being electrically neutral and hydroxyl ion being very low in concentration. On the other hand, the chloride medium acts as an electrolyte, which enable electrical conduction in the solution.

In carbonate and sulphate medium, yellow direct 42 shows the low photoelectrochemical degradation rate (Fig. 13). This result was expected because carbonate and sulphate ions act as radical scavengers (Table 1).

Hydroxyl radical produced are converted to the hydroxide ion thereby decreasing the concentration of these oxidizing agents. As a result, photodegradation process occurs at a very slow rate.

$$SO_4^{2-} + OH^{\bullet} \rightarrow SO_4^{-\bullet} + OH^- \quad (4)$$

Carbonate ions will also react to retransform hydroxyl radical to hydroxide ion as expressed in Eq. (6). However, their scavenging behavior seems less effective compared to sulphate anions or carbonate ions competitive adsorption on ITO thin film may be dominated.

$$HCO_3^- + {}^{\bullet}OH \rightarrow CO_3^{\bullet-} + H_2O \quad (5)$$

$$CO_3^{2-} + {}^{\bullet}OH \rightarrow CO_3^{\bullet-} + OH^- \quad (6)$$

The photocatalytic reaction in the presence of NO_3^- under irradiation of $\lambda < 380$ nm is likely to increase the concentration of hydroxyl radicals as denoted by Eq. (7) [22], and thereby increasing the photodegradation rate.

$$NO_3^- + H_2O + h_{vb}^+ \rightarrow NO_2^{\bullet} + OH^{\bullet} + OH^- \quad (7)$$

However, no clear correlation was found between the rate constant of ions with $^{\bullet}OH$ radical (Table 1) and the order of yellow direct 42 photodegradation in the presence of anions as supporting electrolyte.

Thus, the following order observed for photoelectrocatalytic degradation rate for the selected supporting electrolytes:

$$NaCl > NaNO_3 > Na_2CO_3 > Na_2SO_4$$

The photoelectrochemical characteristic of yellow direct 42 solutions in different supporting electrolyte is shown as linear sweep photovoltametry scans in Fig. 12. Sulphate containing solution showed the lowest anodic photocurrent, while nitrate, carbonate and chloride solutions showed higher values. These behaviors can be explained by the standard half reduction potential for anions listed in Table 2.

The higher the positive potential values, the stronger the oxidizing behavior of the ions. Therefore, solutions containing chloride and nitrate ions show higher photocurrent value than carZbonate and sulphate ions. This is due to the active

Table 2
The half reduction equations and potentials for various types of anions

Half reduction equation	Potential, E (V)	Eq.
$SO_4^{2-} + 4H^+ + 2e^- \rightarrow H_2SO_3 + H_2O$	+0.17	(8)
$Cl_2 + 2e^- \rightarrow 2Cl^-$	+1.36	(9)
$NO_3^- + 2H^+ + e^- \rightarrow NO_2 + H_2O$	+0.80	(10)
$NO_3^- + H_2O + 2e^- \rightarrow NO_2^- + 2OH^-$	+0.10	(11)
$NO_3^- + 4H^+ + 3e^- \rightarrow NO + 2H_2O$	+0.96	(12)
$NO_3^- + 5H^+ + 4e^- \rightarrow 1/2\ N_2O + 5/2H_2O$	+1.11	(13)
$NO_3^- + 6H^+ + 5e^- \rightarrow 1/2N_2 + 3H_2O$	+1.24	(14)
$NO_3^- + 10H^+ + 8e^- \rightarrow NH_4^+ + 3H_2O$	+0.87	(15)

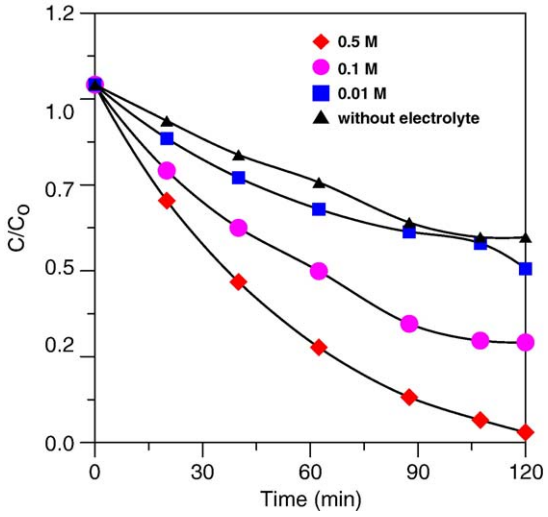

Fig. 14. The photoelectrochemical degradation of yellow direct 42 dependence on the concentration of NaCl (1×10^{-5} mol L^{-1} dye con., pH 5.25 and 450 W Hg lamp irradition).

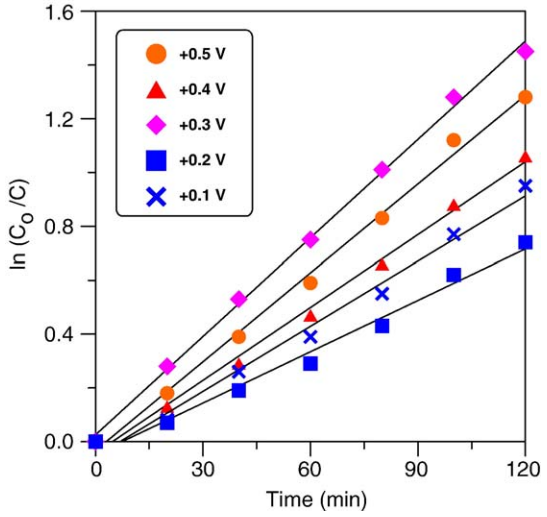

Fig. 15. Dependence of the photoelectrochemical degradation rates on bias potential for the ITO thin-film electrodes in 1×10^{-5} M yellow direct 42 dye of pH 5.25 and 0.5 M NaCl solution under irradition with 450 W Hg lamp.

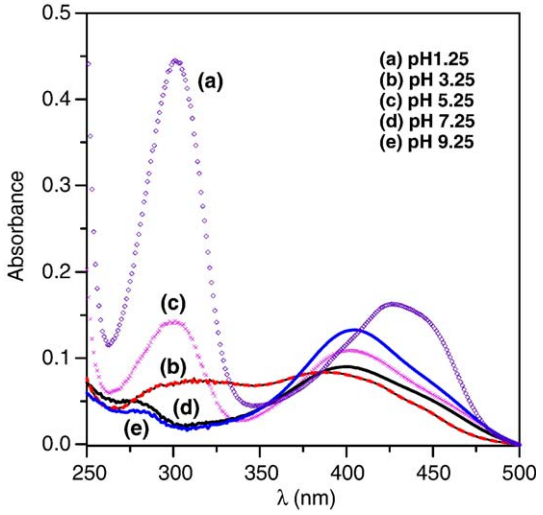

Fig. 17. Effect of pH on UV–Vis absorption spectra of dye solutions of concentration 1×10^{-5} mol L^{-1}.

participation of carbonate and sulphate ions in transformation of hydroxyl radicals to hydroxide ions, which in turn reduce the photodegradation rate.

The dependence of the photoelectrodegradation rate on the NaCl concentration was also presented in Fig. 14, in which the increase in NaCl concentration resulted in the higher photoconversion.

3.6. Effect of applied potential

The effect of applied potential on the photoelectrocatalytic degradation of yellow direct dye was investigated by comparing the color removal during oxidation of 1×10^{-5} mol L^{-1} dye in 0.5 mol L^{-1} NaCl at pH 5.25 in order to check for the importance of selecting the best potential for this process. Potentials ranged between +0.1 and +0.7 V and absorbance decay at 415 nm was monitored over a 120 min. The relationship between $\ln(C_o/C)$ and time for each applied potential is linear. The dependence of the initial degradation rate evaluated from slopes of the curves obtained for dye consumption (mol L^{-1}) as function of time at different potential values is presented in Fig. 15. The initial degradation rates increased from 0.0072 up to 0.0102 min^{-1} through increase in potential between +0.2 and +0.5 V. Further increases in potential lead to a slight increases in degradation.

As calculated from impedance measurements, all of the applied potentials employed in this study are positive to flat band potential (−0.026 V). Therefore, there is always a potential gradient over the ITO film, resulting in an electric field, which keeps photogenerated charges apart. Thus, in all further experiments +0.5 V was chosen as best potential for investigating the degradation of the yellow direct dye.

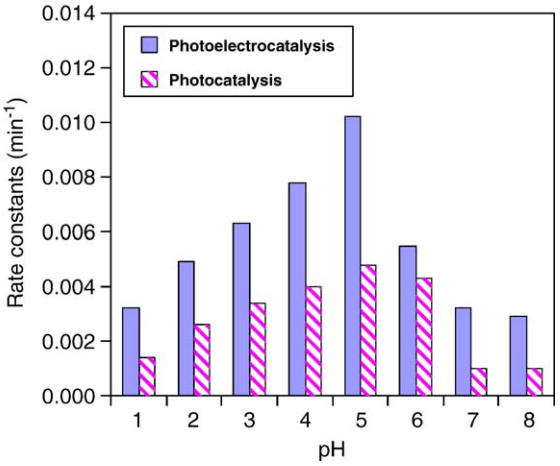

Fig. 16. Effect of pH variation on the initial rate of photoelectrocatalytic and photocatalytic of 1×10^{-5} mol L^{-1} dye on ITO thin-film electrode.

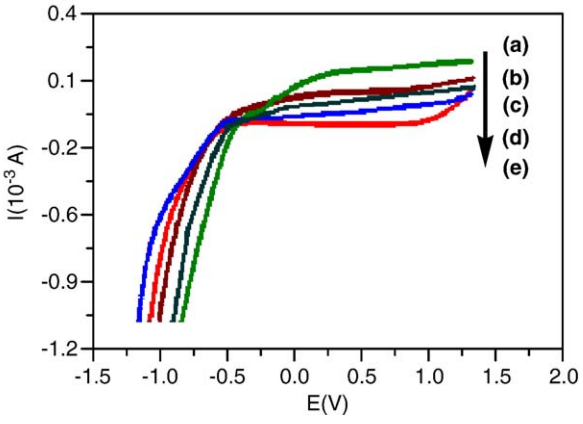

Fig. 18. Photocurrent–potential curves obtained for ITO thin-film electrodes under UV–Vis irradiation (10 mV s^{-1} scan rate and pH 2.25 at various concentration of yellow direct 45 (a) 1×10^{-5}, (b) 2×10^{-5}, (c) 3×10^{-5}, (d) 4×10^{-5}, (e) 5×10^{-5} mol L^{-1}).

3.7. Effect of pH on dye degradation rate

The minority charge carriers photogenerated (h^+) upon illumination on the photoanode can oxidize the adsorbed H_2O/OH^- species producing $^{\bullet}OH$ radicals with the release of H^+ ions to the solution (Eqs. (1), (2) and (3)). Thus, the reaction depends on the pH of the solution [23–26].

$$TiO_2 + h\nu \rightarrow TiO_2{-}e^-_{cb} + TiO_2{-}h^+_{vb} \quad (16)$$

$$TiO_2{-}h^+_{vb} + H_2O_{(ads)} \rightarrow TiO_2{-}OH^{\bullet}_{(ads)} + H^+ \quad (17)$$

$$TiO_2{-}h^+_{vb} + OH^-_{(ads)} \rightarrow TiO_2{-}OH^{\bullet}_{(ads)} \quad (18)$$

The photoelectrochemical and photocatalytic degradation rates of yellow direct 42 dye were investigated in solutions of various pH. The results are presented in Fig. 16. It is found that the best photodegradation results are obtained within acidic medium. Fig. 17 shows the effect of pH on the UV–Vis spectra of dye solutions.

3.8. Effect of dye concentration

The influence of the initial concentrations of yellow direct 42 dye on the photoelectrocatalytic degradation was investigated by keeping constant all previously optimized parameters. Dye concentration is ranged from 1×10^{-5} to 5×10^{-5} mol L^{-1}. The photoelectrocatalytic degradation of the dye in 0.5 mol L^{-1} NaCl pH 5.25 at $E=+0.5$ V was followed by measuring the absorbance decay at $\lambda=415$ nm over 120 min. The degradation rates evaluated from the linear relationship of $\ln(C_o/C)$ versus t decreases from 0.0102 min^{-1} (1×10^{-5} mol L^{-1}) to 5.1×10^{-3} min^{-1} (5×10^{-5} mol L^{-1}). To investigate this phenomenon further, the influence of dye concentration on the photocurrent obtained from linear sweep voltammograms recorded at the ITO thin film electrode in NaCl 0.5 mol L^{-1} was investigated and presented in Fig. 18 (curves (a–e)). The photocurrent decreases markedly when dye concentration is increased in solution. As the oxidation reaction occurs by the hydroxyl radical generated via surface bound hydroxyl groups adsorbed, the competition of dyes molecules at higher concentration leads to a decrease in the rate of degradation. In addition, at higher concentration, the light intensity reaching the ITO thin film surface is reduced due to the lower transparency of the solution or the quantity of intermediates increased as well, competing through side reactions with the dye decomposition [27,28].

4. Conclusion

Photoelectrocatalytic oxidation of an azo-dye solution can be achieved efficiently using thin-film ITO photoanodes and UV irradiation. The results indicate the importance of the operational parameters towards obtaining high photoelectrochemical degradation rate. The control of pH solutions (acidic media), yellow direct 42 concentration (1×10^{-5} mol L^{-1}), applied potential (+0.5 V) and annealing temperature (550 °C) are resulted to enhance the efficiency of this process. Addition of a small amount of supporting electrolyte influenced the dye degradation performance. Chloride and nitrate ions promote the degradation rate while sulphate and carbonate ions show opposite effect. The mechanism of the reactions taking place during the photodegradation process is based on the electron-hole pair generation and heterogeneous oxidation with participation of valence-band holes. The reactions with h_{vb} involve oxidation of solution components with generation of powerful oxidants, such as the $^{\bullet}OH$, $Cl_2^{\bullet-}$ and $Cl^{\bullet}$ radicals, being directly responsible for the fast dye decomposition.

Acknowledgment

The authors wish to thank the University of Isfahan for financially supporting this work.

References

[1] A. Fujishima, T.N. Rao, D.A. Tryk, J. Photochem. Photobiol., C Photochem. Rev. 1 (2000) 1.
[2] K. Pirkanniemi, M. Sillanpaa, Chemosphere 48 (2002) 1047.
[3] K. Shaw, P. Christensen, A. Hamnett, Electrochim. Acta 41 (1996) 719.
[4] M.A. Fox, M.T. Dulay, Chem. Rev. 93 (1993) 341.
[5] D. Chen, A.K. Ray, Water Res. 32 (1998) 3223.
[6] J.A. Bryne, B.R. Eggins, N.M.D. Brown, B. McKinney, M. Rouse, Appl. Catal., B Environ. 17 (1998) 25.
[7] M.R. Hoffman, S.T. Martin, W.Y. Choi, D.W. Bahnemann, Chem. Rev. 95 (1995) 69.
[8] J.A. Bryne, A. Davidson, P.S.M. Dunlop, B.R. Eggins, J. Photochem. Photobiol., A Chem. 148 (2002) 365.
[9] R.L. Pozzo, M.A. Baltanas, A.E. Cassano, Catal. Today 39 (1997) 219.
[10] A. Blozkow, I. Csolleova, V.J. Brezova, J. Photochem. Photobiol., A Chem. 113 (1998) 251.
[11] C.M.A. Brett, A.M.O. Brett, Electrochemistry: Principles, Methods and Applications, Oxford University Press, Oxford, 1993.
[12] D.T. Sawyer, J.R. Roberts, Experiments for Chemists, Wiley, New York, 1974.
[13] K. Kato, A. Tsuzuki, Y. Torii, H. Taoda, J. Mater. Sci. 30 (1995) 837.
[14] K. Kato, A. Tsuge, K. Niihara, J. Am. Ceram. Soc. 79 (1996) 1483.
[15] K. Kato, K. Niihara, Thin Solid Films 29 (1997) 76.
[16] M.V.B. Zanoni, J.J. Sene, M.A. Anderson, J. Photochem. Photobiol., A Chem. 157 (2003) 55.
[17] J. Luo, M. Hepel, Electrochim. Acta 46 (2001) 2913.
[18] B.D. Cullity, Elements of X-ray Diffraction, 2nd ed., Addison-Wiley, MA, 1978.
[19] W.M. Shen, M. Tomkiewicz, D. Sedaies, C. Levy-Clement, J. Electrochem. Soc. 137 (1990) 2656.
[20] R. Andreozzi, V. Caprio, A. Insola, R. Marotta, Catal. Today 53 (1999) 51.
[21] R.J. Candal, W.A. Zeltner, M.A. Anderson, Environ. Sci. Technol. 34 (2000) 3443.
[22] S. Murakami, T. Yoshino, Polyhedron 1 (1982) 405.
[23] Y. Katsumura, J. Phys. Chem. 95 (1991) 4435.
[24] G.V. Buxton, C.L. Greenstock, W.P. Helman, A.B. Ross, J. Phys. Chem. Data 17 (1988) 513.
[25] J. Holcman, T. Logager, K. Sehested, V. Klaning, Laboratory Studies on Atmospheric Chemistry, Springer, New York, 1991.
[26] B. Lesigne, C. Ferradini, J. Pucheault, J. Phys. Chem. 76 (1972) 24.
[27] K. Ogura, S. Kurakami, K. Seneo, J. Inorg. Nucl. Chem. 43 (1981) 1243.
[28] T.M. Florence, J. Electroanal. Chem. 52 (1974) 115.